Supplemental information

Shape of fractional volume curve

Examples of the shapes of the curves defined by Equation 18 are shown as the solid lines in Figure S1. The curves begin at values $v_i = v_{i0}$ and have asymptotic or equilibrium values $v_i \rightarrow n_i$ for $t \rightarrow \infty$ or $\tau \rightarrow \infty$ (shown as horizontal lines in Figure S1; these values correspond to the droplets reaching equal solute concentrations on each side of the bilayer). The curves don't cross if the larger droplet has the higher fraction of solute (Case I with $n_i > n_j$ when $v_i > v_j$, shown in Figure S1a) and cross if the larger droplet has the smaller fraction of solute (Case II with $n_i < n_j$ when $v_i > v_j$, shown in Figure S1b). Figure S1 shows v_{10} and v_{20} with their extremal values 0 and 1. For either case, there is only one curve shape for any given value of n_i; the curve for the second droplet is a vertical reflection of the first curve through the value 0.5 (i.e., $v_i = 1\text{-}v_j$), and curves starting at different v_{i0} simply start at different points on the curve.

Although the curves in Figure S1 appear to be exponential, an exponential curve is in fact a poor approximation to the correct shape. The nonlinearity in Equation 18 introduces the quadratic correction that leads to an infinite slope for dv_i/dt for the limiting cases of v_{i0} or $v_{j0} \rightarrow 0$, where the concentration gradient becomes infinite for non-zero n_i. This distinction from an exponential is seen from the dashed curves marked Q and E in Figure S1, which show the quadratic portion described by the first two terms (a parabola) in Equation 18, and a true exponential described by the third term in Equation 18, respectively. The correct values of τ (solid lines) are the sum of these two curves. The maximum contribution of the quadratic term to $P\tau$ occurs at $[n_i , -(v_{i0} - n_i)(v_{i0} + n_i - 2\, n_j)/2]$ for v_i in Case I and at the vertex of the parabola at $[n_j , -(v_{i0} - n_i)^2/2]$ for v_i in Case II. A comparison of Equation 18 with our experimental results is described in the Results section.

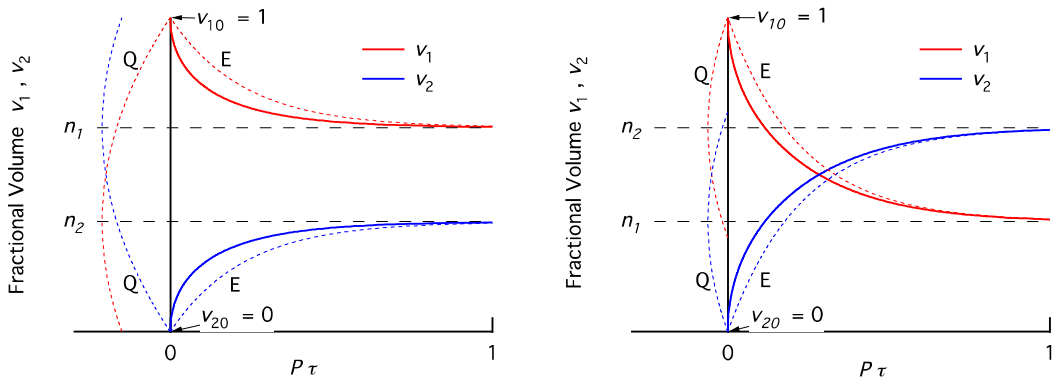

Figure S1. Shapes of curves for volume ratio as a function of the time-like variable $P\tau$ for (a) Case I with $n_i > n_j$ for $v_i > v_j$, and (b) Case II with $n_i < n_j$ for $v_i > v_j$.

Droplet Pair With Delayed Equilibrium Bilayer Conditions

Figures S2 through S7 show data for a droplet pair that shows a delay in attainment of the equilibrium bilayer conditions. Although there are large changes in the center-to-center distance, bilayer contact angle, and bilayer radius between roughly 5 and 9 ks, no dramatic changes are seen in the droplet radii and droplet volumes (Figures S2 through S4). Similarly, the permeability appears to have the same value before and after this transition (i.e., from ~2-5 ks and after ~9 ks; see Figures S5 and S6). However, during the transition, the permeability appears to deviate from the final value (Figures S5 and S6). It is not clear whether this is a true deviation or an artifact of the permeability calculation. This change disturbs the fit using Equation 18 (see Figure S7).

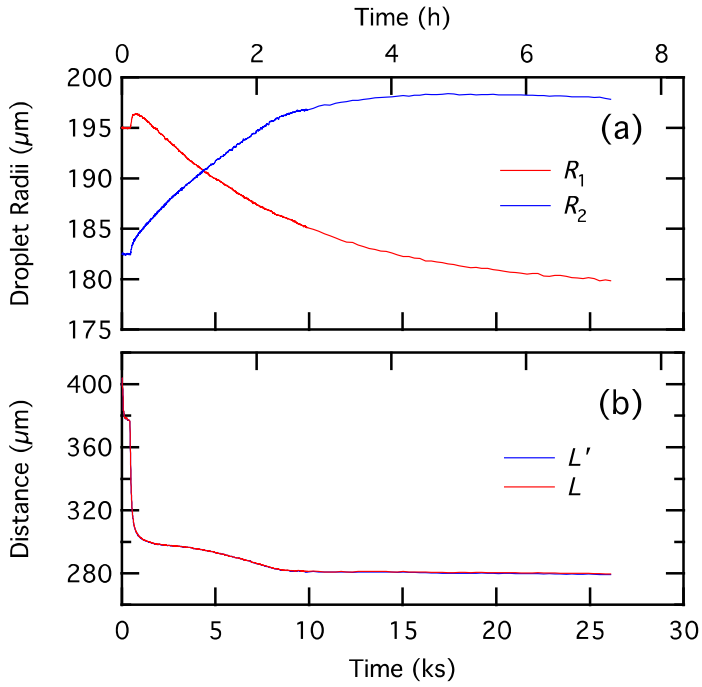

Figure S2. Raw data (droplet radii and center-to-center distance) versus time for droplet pair with delayed equilibrium.

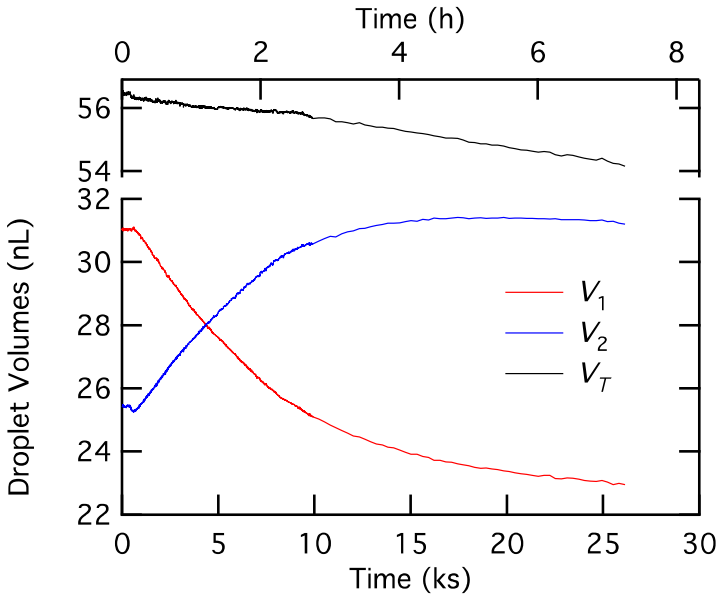

Figure S3. Droplet volumes versus time for droplet pair with delayed equilibrium.

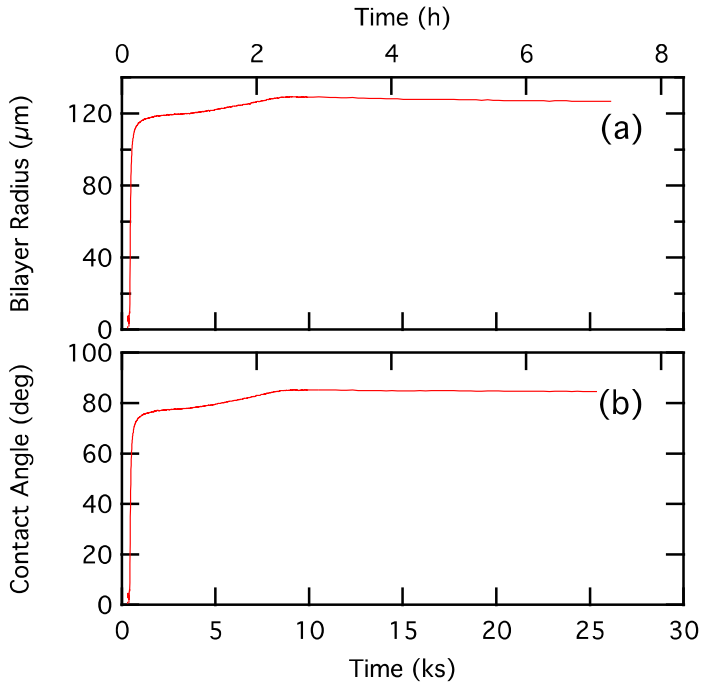

Figure S4. Droplet bilayer radius and contact angle versus time for droplet pair with delayed equilibrium.

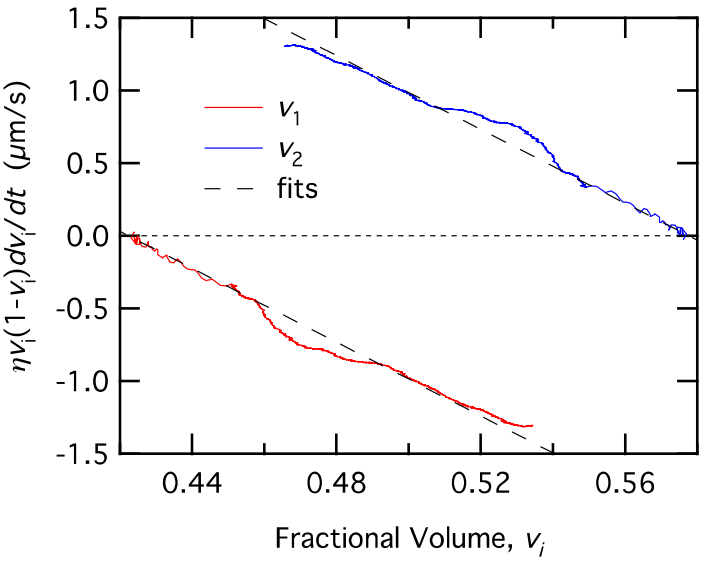

Figure S5. Data and fits using Equation 16 for droplet pair with delayed equilibrium.

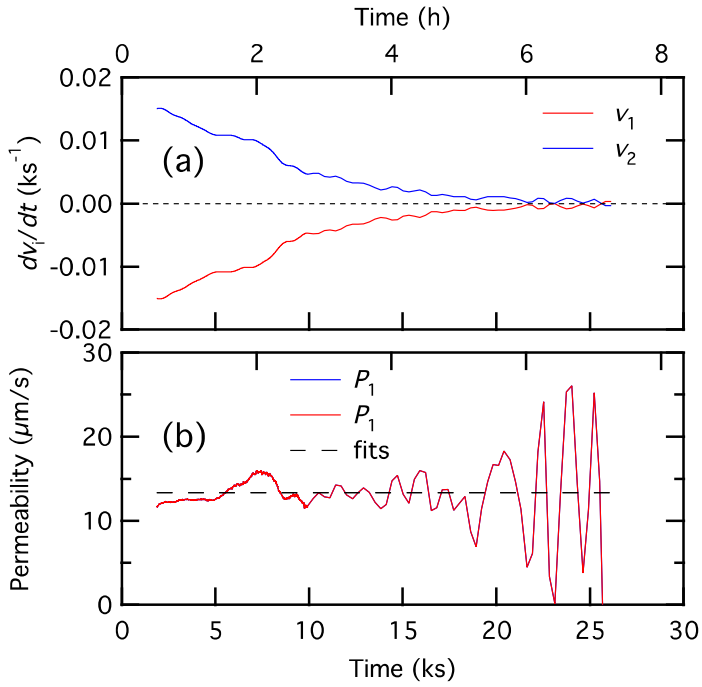

Figure S6. Plot of dv_1/dt (a) and P (b) as a function of time for droplet pair with delayed equilibrium.

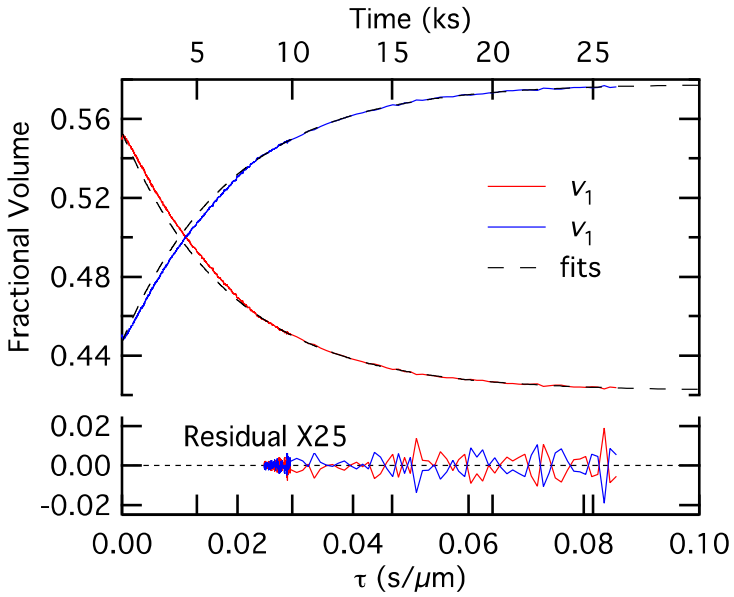

Figure S7. Plot of dv_1/dt (a) and P (b) as a function of time for droplet pair with delayed equilibrium.